The Astronomical Journal, 166:211 (15pp), 2023 November https://doi.org/10.3847/1538-3881/acffb7

A Study of Eight Visual-spectroscopic Southern Binaries Using Recent SOAR Observations

José A. Docobo[1,2], Pedro P. Campo[2], Jorge Gómez[2], René A. Méndez[3], and Edgardo Costa[3]
[1] Centro de Investigación e Tecnoloxía Matemática de Galicia Rúa de Constantino Candeira s/n, Campus Vida, Santiago de Compostela, E-15782, Galiza, Spain joseangel.docobo@usc.es
[2] Observatorio Astronómico Ramón María Aller, Universidade de Santiago de Compostela (USC), Avenida das Ciencias s/n, Campus Vida, Santiago de Compostela, E-15782, Galiza, Spain; pcampodiaz@gmail.com
[3] Universidad de Chile, Casilla 36-D, Santiago, Chile; rmendez@uschile.cl
Received 2023 August 9; revised 2023 September 30; accepted 2023 October 2; published 2023 October 27

Abstract

Speckle observations performed between 2019 and 2022 with the HRCam attached to the 4.1 m SOAR telescope (Cerro Pachón, Chile) permitted to improve visual orbits of the southern binaries WDS 01243-0655 (BU 1163), WDS 09275-5806 (CHR 240), WDS 12114-1647 (S 643 AaAb), WDS 13317-0219 (HDS 1895), WDS 15282-0921 (BAG 25 AaAb), WDS 17304-0104 (STF 2173), WDS 19598-0957 (HO 276), and WDS 21274-0701 (HDS 3053). All of them are spectroscopic binaries, of which six are SB2, so relevant information about their individual masses has been obtained. Moreover, comparison between different values of their parallaxes (orbital, dynamic, and ANAPAR, a color-dependent model suitable for binary systems attending to the exact locations of the components on the MS in the HR diagram) with those provided by Hipparcos and Gaia missions, along with comments for each binary are presented. The luminosity determination of the 16 components allowed us to estimate their approximate age and position on the HR diagram as well.

Unified Astronomy Thesaurus concepts: Orbit determination (1175); Orbits (1184); Stellar astronomy (1583); Stellar dynamics (1596); Stellar evolutionary tracks (1600); Stellar masses (1614); Stellar parallax (1618); Binary stars (154); Visual binary stars (1777); Spectroscopic binary stars (1557)

1. Introduction

It is well known that double and multiple stars represent a fundamental source of astronomical information, not only because we can determine the masses of the components from their orbits, which in itself is a very important motivation for their study, but also because such stellar systems allow to research multiple physical and dynamical phenomena: Keplerian and perturbed orbits, multiple stellar systems, establishing the mass–luminosity relationship, orbital and dynamical parallaxes, influence of radiation induced mass loss and transference, variable components of different kinds, magnetic binaries, etc.

In the 1970s a new technique for the optical observation and identification of new components appeared. Speckle interferometry (Labeyrie 1970) has allowed the obtaining astrometric positions and differential photometry with unprecedented precision. Mainly used in class 4–6 m telescopes, it was at that moment a true revolution in this field of research that reaches our time accompanied by adaptive optics and long baseline interferometry.

By means of speckle interferometry, it is possible to overcome the limits imposed by the atmospheric seeing and achieve resolutions close to the diffraction limit of the telescope. This allowed several groups to resolve optically several spectroscopic binaries (see, for example, McAlister 1976, 1977, 1978; Balega et al. 1984; Barlow et al. 1993; Pourbaix 1998). This fact was specially important for the determination of three-dimensional orbits, and therefore the deduction of the orbital parallaxes and the individual masses.

Another quality leap happened twenty years later with the launch of the astrometric satellite, Hipparcos (Perryman et al. 1997; van Leeuwen 2007). This satellite yielded parallaxes that, in many cases, were vastly superior to those obtained from the ground, which improved the precision of the calculated stellar masses, besides providing many measured parameters, the detection of astrometric orbits, and photometric and astrometric information. Nowadays in the Gaia era (Gaia Collaboration et al. 2016, 2018, 2023) all the astronomical research, and in particular binary stars, have reached a golden age, mainly after the data releases DR2, EDR3, and DR3, and with the prospect of all the information available in the full catalog expected for 2030.

The use of large ground-based telescopes with modern detectors, along with the observational data from the space telescopes enables the future research of double and multiple systems from different points of view. Among the active telescopes for the observation of binaries in the southern hemisphere it is the Southern Astrophysical Research telescope (SOAR). The research included in this article is based on recent observations made with the HRCam attached to this 4.1 m telescope, within the collaboration established between the Universities of Chile and Santiago de Compostela through the Ramón María Aller Astronomical Observatory.

The "Speckle Interferometry at SOAR" series (hereafter, TMH10; Tokovinin et al. 2010a, 2010b, 2015, 2016, 2018, 2019, 2020, 2021, 2022; Tokovinin 2012) explains the characteristics and results of the different observational Speckle interferometry programs that had been developed during more than a decade and a half in SOAR.

Table 1
Magnitudes and Spectral Types

Washington Double Star Catalog (WDS)	Magnitudes		Spectral types			References Spectral Types
	A	B	Combined	A	B	
01243-0655	6.59	6.98	F4V	F3V	F6V	Abt (2009)
09275-5806	7.65	8.33	G2V	G0V	G6.5V	Houk & Cowley (1975)
12114-1647	7.54	8.23	G6V	G3V	G9V	Gray et al. (2006)
13317-0219	7.65	9.48	G9V	G5.5V	K3V	Frasca et al. (2009)
15282-0921	6.93	10.42	G9V	G8V	M0V	Gray et al. (2003)
17304-0104	6.06	6.10	G5V	G4.5V	G5V	Sharma et al. (2020)
19598-0957	6.22	7.83	F9V	F6V	G8V	Gray et al. (2003)
			G2V	F9.5V	K1V	Houk & Swift (1999)
21274-0701	7.97	9.14	G0V	F8.5V	G8V	Houk & Swift (1999)

Note. This table concerns the magnitudes and the spectral type of each component of the eight binaries studied. In column 1 the Washington Double Star Catalog (WDS) number appear. Columns 2 and 3 correspond to the apparent magnitudes for the components principal (A) and secondary (B). Columns 4 lists the combined spectrum, columns 5 and 6 includes the calculated individual spectral types for the components A and B, respectively, and column 7 the reference for the combined spectrum.

Those campaigns had been developed using the HRCam (Tokovinin & Cantarutti 2008) working at the 4.1 m SOAR telescope (Sebring et al. 2003). Information regarding the reduction of the data blocks and the astrometrical and photometrical resolution of the systems observed can be obtained in Tokovinin (2018a) and references therein. The nominal diffraction-limited resolution, i.e., the diffraction limit $\frac{\lambda}{D}$, is 27 mas at 540 nm wavelength and 40 mas at 800 nm. Standard magnitude limit is $I \approx 12$ mag under typical seeing, although pairs as faint as I $\approx$ 16 mag can be measured under exceptionally good seeing but with less accuracy and resolution.

We present a study of eight visual binaries, which were tracked by means of speckle interferometry, and that also have a spectroscopic orbit, six of them SB2. Seven of this orbits were obtained from the 9th Catalogue of Spectroscopic Binary Orbits[4] and one from the Gaia Archive (the DR3 two body orbit catalog). Apart from a fine-tuned improvement of their visual orbits shown in the lower rms in θ and ρ, we describe thoroughly the determination of the individual masses of each component and the different parallaxes, comparing our results with those previously deduced by other authors for the same objects.

In order to perform the orbit calculation, in the last decades different methods (Thiele-Innes-Van den Bos, Zwiers, Kowalsky, in Zwiers 1896; Vidal 1953; Cid 1958, 1960; Heintz 1978; Docobo 1985, 2012; Catovic & Olevic 1992; Olević & Cvetković 2004), and new optimization techniques to minimize the residuals between observed and calculated positions have been used (Monet 1979; Hartkopf et al. 1989; Wales & Doye 1997; Pourbaix 1998; MacKnight & Horch 2004; Branham 2005; Tokovinin 2016a; Mendez et al. 2017, among others). On our behalf, we have tried not only that the rms in θ, ρ, and even the radial velocities are minimal, but also that the sequence of signs of the residuals is well distributed, avoiding systematic errors. In this sense, we have used the analytical method of Docobo (Docobo 1985, 2012) in order to calculate a preliminary solution which is later improved by a least squares minimization. Finally, if it is necessary, the method of Docobo is applied again for a final adjustment to avoid systematical deviations, even if they are small. Logically, a previous step consists in assigning a weight to each observation depending on the technique and the telescope utilized. The scheme for the micrometric observations can be seen in Docobo & Ling (2003); whereas, for the interferometric observations, the weights are assigned according to the aperture of the telescope because the size of the pixel in the speckle cameras decreases when the aperture increases, therefore improving the resolution: 5 for apertures smaller than 1 m, 10 for 1–2 m, 15 for 2–3 m, 20 for 3–4 m, 25 for 4–5 m, 30 for 5–6 m, and 35 for larger apertures.

As it is well known, the method of Docobo, based on the obtaining of a set of relative orbits that apparent orbits pass through three selected points, without the need for the calculation of the areal constant, permits to choose the best orbit according to different criteria, not only the minimal rms, but also the proximity of the dynamical parallax for each of the orbits, calculated using both the classical Baize–Romani algorithm (Baize & Romani 1946; herein designated as dynamical) and the ANAPAR procedure (Andrade 2019), to those from Hipparcos and Gaia. Another criterion may be the comparison of the individual masses deduced from the dynamical and ANAPAR parallaxes with the typical masses that correspond to the spectral types of the components.

The individual spectral types were determined by means of the method of Edwards (Edwards 1976; Campo 2019) from the combined spectrum and the magnitude difference between the components, Δm. The first were taken from Houk & Cowley (1975), Houk & Swift (1999), Gray et al. (2003, 2006), Abt (2009), Frasca et al. (2009), and Sharma et al. (2020; see Table 1); whereas, for Δm, unless the individual magnitudes are available, we took the mean of the values in the V band from the speckle results of each binary.

Another useful tool that we have used in the present research, is the algorithm to obtain the three-dimensional orbit of a spectroscopic binary with one speckle measurement and the parallax (Docobo et al. 2014). This algorithm also permits to study the coherence of the available speckle measurements in each case. We will refer to it in the text as the 3D methodology.

After this introduction, in Section 2 the results and the comments for each binary are presented.

In Section 3 we have calculated the absolute magnitudes and luminosities (see Table 8) with the aim of determining the position of the different objects in the HR diagram and plotting

[4] https://sb9.astro.ulb.ac.be/

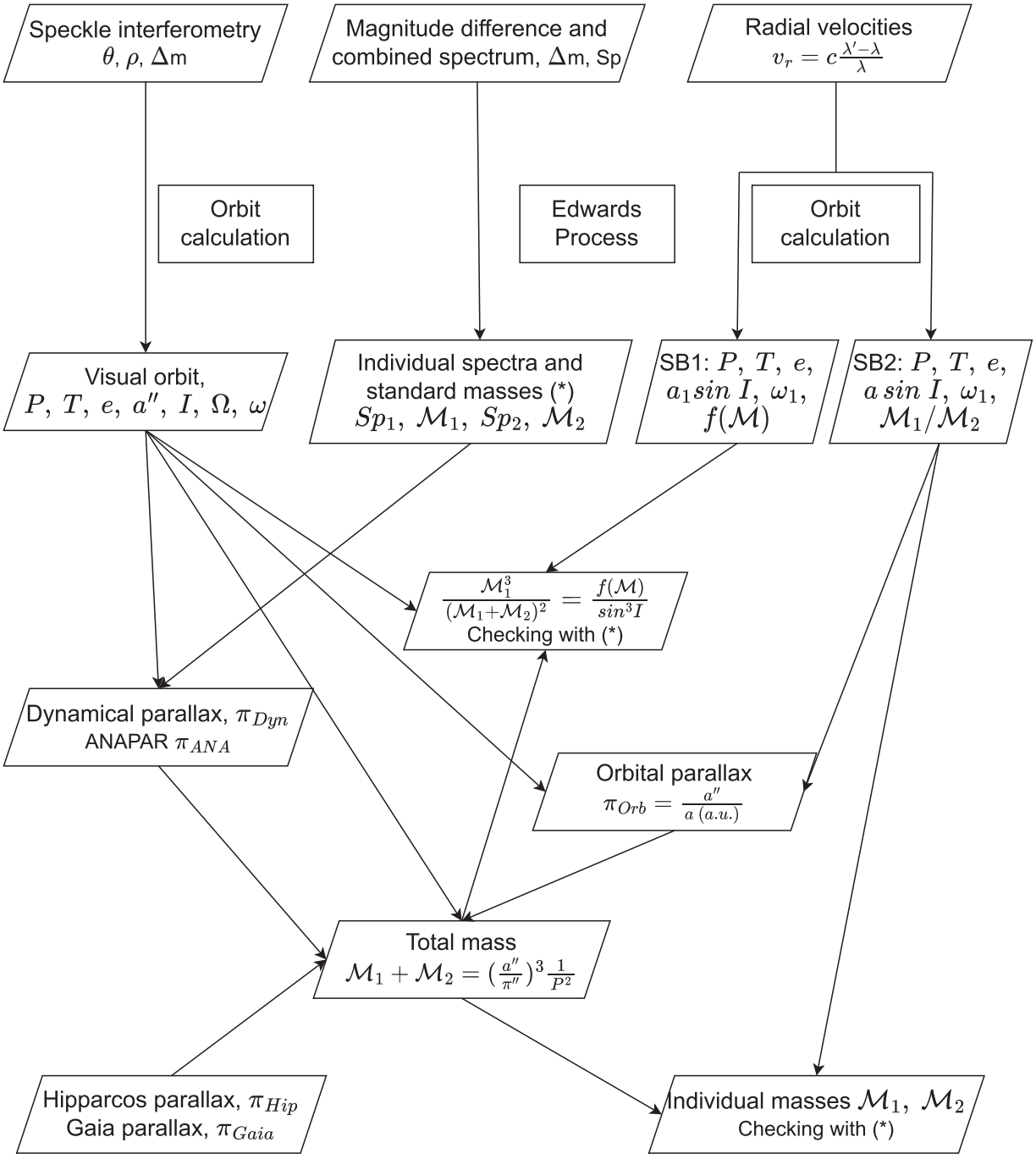

Figure 1. Flowchart of the calculation process.

the isochrones with MIST (Paxton et al. 2011, 2013, 2015; Choi et al. 2016; Dotter 2016). The parallaxes that we used have been the ANAPAR parallaxes.

Seven of the orbits studied had been announced in the IAUDS Circular No 207 (Docobo et al. 2022), and that of the system BU 1163 in No 209 (Docobo et al. 2023).

2. Results and Discussion

In Figure 1 a flowchart of the methodology used to obtain the results is presented. We calculate a visual orbit from all the visual and interferometric measurements available, checking their compatibility with the published spectroscopic orbits and the rms error of the difference between the observations and the calculated positions. At the same time, using the combined spectrum and the magnitude difference, we apply the Edwards process to obtain the individual spectra, which in turn provide the standard masses of the components through calibrations such as the one in Pecaut & Mamajek (2013). This masses represent an additional check for the fitness of the orbit. The visual orbit, along with the spectral decomposition and the magnitudes are used to calculate the dynamical and ANAPAR parallaxes, and for stars with SB2 orbits, we can calculate the orbital parallax from a'', and a in astronomical units, which in turn can be determined by using a sin I from the spectroscopic orbit and I from the visual orbit. The different parallaxes, combined with the visual orbit, by means of Kepler's Third

Table 2
Orbital Elements of the Visual Orbits

WDS Name	P (yr) σ	T (Besselian) σ	e σ	a (arcsec) σ	I (°) σ	Ω(°) σ	ω(°) σ	T (Julian) Last Observation
01243-0655	16.046	2021.134	0.929	0.1996	117.0	28.9	348.6	2021.132
BU 1163	± 0.224	± 0.008	± 0.003	± 0.0010	± 0.5	± 0.5	± 0.5	2021.7556
09275-5806	1.4164	2023.8894	0.3761	0.0335	131.19	81.63	327.71	2022.471
CHR 240	± 0.0049	± 0.0210	± 0.0018	± 0.0001	± 2.65	± 1.03	± 0.55	2022.2825
12114-1647	0.5792	2018.732	0.2911	0.0261	39.44	234.22	103.59	2018.730
S 634 AaAb	± 0.0005	± 0.006	± 0.0009	± 0.0010	± 1.50	± 1.50	± 0.50	2021.2451
13317-0219	3.240	2023.512	0.528	0.0969	20.4	129.2	179.4	2023.510
HDS 1895	± 0.008	± 0.002	± 0.002	± 0.0015	± 0.5	± 1.5	± 1.5	2021.1602
15282-0921	2.4363	2024.315	0.9735	0.1052	55.73	96.51	72.62	2024.317
BAG 25 AaAb	± 0.0018	± 0.022	± 0.0017	± 0.0025	± 0.48	± 1.48	± 1.36	2022.2827
17304-0104	46.52	2055.36	0.171	0.9679	99.5	331.9	146.7	2055.36
STF 2173	± 1.50	± 0.50	± 0.004	± 0.0011	± 0.5	± 0.5	± 2.5	2021.2454
19598-0957	4.8705	2026.628	0.6015	0.1518	17.32	154.19	132.15	2026.623
HO 276	± 0.0030	± 0.0010	± 0.0035	± 0.0004	± 1.50	± 8.00	± 8.00	2019.3734
21274-0701	20.645	2036.419	0.360	0.1639	50.2	153.4	148.9	2036.417
HDS 3053	± 0.300	± 0.250	± 0.005	± 0.0020	± 1.0	± 1.0	± 1.0	2020.8339

Note. We Identified in the first column each binary by its WDS number and by the discoverer code, which is the name of the binary, and the corresponding orbital elements with their standard errors (Columns 2–8): the period, P, in years; the time of the periastron passage, T, in Besselian years; the eccentricity, e; the semimajor axis, a, in arcseconds; the inclination, I; the angle of the node, Ω; and the argument of the periastron, ω, the last three in degrees. The periastron passage, T, expressed in Julian years and the date of the last observation used in the calculation of the orbit are included in column 9. Previously to the calculation of the orbits, the observations were corrected for precession in order to refer the position angles to the standard equinox of J2000.0.

Table 3
Rms Quality Controls Compared to the Previous Orbits

		This paper		Previous Orbits[a]		
		rms		rms		(Author)
WDS	Name	$\Delta\theta$	$\Delta\rho$	$\Delta\theta$	$\Delta\rho$	
01243-0655	BU 1163	2.271	0.0151	4.208	0.0151	Söderhjelm (1999)
09275-5806	CHR 240	4.351	0.0039	5.873	0.0039	Tokovinin (2016b)
12114-1647	S 634 AaAb	1.700	0.0028	2.807	0.0034	Tokovinin (ORB6)
13317-0219	HDS 1895	1.503	0.0028	2.045	0.0028	Tokovinin et al. (2020)
15282-0921	BAG 25 AaAb	5.236	0.0053	5.294	0.0053	Anguita-Aguero et al. (2022)
17304-0104	STF 2173	2.640	0.0615	2.797	0.0628	Pourbaix (2000)
19598-0957	HO 276	1.643	0.0064	2.028	0.0069	Tokovinin (2017)
21274-0701	HDS 3053	1.398	0.0030	1.433	0.0030	Mitrofanova et al. (2021)

Notes. In the present table, the weighted rms of the differences between the observed and the calculated values of the θ and ρ coordinates to compare the orbits that we calculate with the last determined are shown. Columns 1 and 2 identify the binary by its WDS number and the name of the binary. Columns 3 and 4 list the rms in θ and ρ obtains with the orbits presented in this paper, and columns 5 and 6 the same rms now deduced using the last orbit, which were calculated by the authors listed in column 7.
[a] We list only the last orbit.

Law, give the sum of the masses of the components, and even the individual masses in the case of the dynamical and ANAPAR parallaxes. For the SB2, the mass sum and the mass ratio yield the individual masses, and for the SB1 we can obtain them from the mass sum, the mass function from the spectroscopic orbit, and the inclination from the visual orbit.

All the information regarding the orbital elements, ephemeris, quality controls of the orbits, parallaxes and masses is included in Tables 1–6. The values of the parallaxes are also represented in Figure 2. Figures 3–10 show the apparent orbits as well as the available observations. The details of the figures can be seen in the caption of Figure 3.

2.1. WDS 01243-0655 (BU 1163, HIP 6564, HD 8556)

This binary was discovered by S. W. Burnham in 1890 (Aitken & Doolittle 1932), and both its components have similar brightness and color, as evidenced by their magnitude difference and spectral types.

Table 4
Orbital Elements of the Spectroscopic Orbits (Only the Last Orbit)

WDS name	P (day) σ	T (RJD) σ	e σ	ω_1(°) σ	K_1(km s^{-1}) σ	K_2(km s^{-1}) σ	γ(km s^{-1}) σ	Reference
01243-0655 BU 1163	5895.01	41588.76	0.92	0.0	40.1[a]			(1)
09275-5806 CHR 240	513.675 ± 0.694	57171.455 ± 1.679	0.3966 ± 0.0116	327.53 ± 4.96	3.020 ± 0.146		10.486 ± 0.074	(2)
12114-1647 S 634 AaAb	211.585 ± 0.029	58383.709 ± 0.270	0.281 ± 0.002	284.0 ± 0.5	15.484 ± 0.039	17.706 ± 0.039	2.369 ± 0.020	(3)
13317-0219 HDS 1895	1188.0 ± 9.0	49474.8 ± 5.6	0.641 ± 0.027	355.8 ± 3.9	3.14 ± 0.16		−51.148 ± 0.072	(4)
15282-0921 BAG 25 AaAb	889.813 ± 0.017	47967.519 ± 0.015	0.9733 ± 0.0006	252.64 ± 0.73	36.42 ± 0.38	52.90 ± 1.73	7.47 ± 0.20	(5)
17304-0104 STF 2173	16924.4 ± 7.7	37897.97 ± 56.68	0.1678 ± 0.0025	328.7 ± 1.3	4.94 ± 0.11	5.32 ± 0.12	−77.181 ± 0.069	(6)
19598-0957 HO 276	1786.27 ± 1.68	45259.4 ± 7.1	0.5927 ± 0.0058	319.8 ± 2.9	4.69 ± 0.13	4.64 ± 0.28	29.683 ± 0.076	(7)
21274-0701 HDS 3053	7576 ± 14	57262.8 ± 9.8	0.363 ± 0.003	324.4 ± 0.7	3.34 ± 0.15	8.66 ± 0.14	−0.75 ± 0.14	(8)

Notes. The orbital elements of the spectroscopic orbits that had been calculated for the eight binaries studied in this research are included in this table. In order to simplify the information, only the last orbit has been included. In this table, column 1 includes the identifications of each binary in the same mode as the previous tables, that is to say, the WDS number and the name of the binary star. Columns 2–8 give information of the orbital elements of each spectroscopy binary with the corresponding standard errors: the period, P, in days; the periastron passage, T, in reduced Julian days; the eccentricity, the argument of the periastron of the primary, ω_1 ($|\omega_1 - \omega| = 180°$); the RV amplitude of the primary; the RV amplitude of the secondary; and the velocity of the center of masses. Column 9 provides the reference of each spectroscopic orbit.

[a] Although this is an SB2 system, the authors give $K_1 + K_2$.

References. (1) Fletcher (1973), (2) Gaia Collaboration et al. (2016, 2023), (3) Tokovinin (2019), (4) Latham et al. (2002), (5) Halbwachs et al. (2018), (6) Pourbaix (2000), (7) Pourbaix (2000), (8) Tokovinin (2018b).

The first orbits as a visual binary were calculated by W. H. Van den Bos (van den Bos 1934), but by then it was not clear if the orbital period was close to 16 yr or double than that. In the first case it would be a very eccentric orbit, whereas in the second it would be nearly circular. New orbits were obtained later by the same author, in 1956 for both possible periods, and in 1962 for 16 yr (van den Bos 1956, 1962).

In 1973, Fletcher (1973) determined the first (SB2) spectroscopic orbit using 12 measurements of radial velocities obtained by himself and other authors. Previous spectroscopic observations reported by Evans (1957) and Ishida (1966) did not show enough duplicity of the spectral lines. This orbit showed that the real solution was the one with short period.

New orbits were calculated later by several authors based only on visual measurements (Finsen 1973; Morbey 1975; Starikova 1978; Hartkopf et al. 1996; Söderhjelm 1999), which improved the previous orbits but now show large errors for the newer observations.

Since the 1970s, this binary has been followed by means of speckle interferometry, mainly by H. A. McAlister (McAlister & Degioia 1979; McAlister & Fekel 1980; McAlister & Hendry 1982; McAlister et al. 1983; McAlister & Hartkopf 1984; McAlister et al. 1987; Al-Shukri et al. 1996; Fu et al. 1997), W. Hartkopf (Hartkopf et al. 1992, 1993, 1996, 1997, 2000), B. D. Mason (Mason et al. 1999; Douglass et al. 2000; Mason et al. 2001a, 2001b, 2002, 2009), E. Horch (Horch et al. 1999, 2000, 2001a, 2001b, 2002, 2004, 2006a, 2006b; Davidson & Baptista 2009; Horch et al. 2011), and A. Tokovinin (Tokovinin 1982, 1983, 1985; Tokovinin & Ismailov 1988; Tokovinin et al. 2010a, 2010b; Hartkopf et al. 2012; Tokovinin et al. 2015), which has allowed to obtain increasingly accurate orbits. Our visual solution is based on the last measurements carried out by Tokovinin et al. (2020) at SOAR. A comparative between the rms in θ and ρ of the last orbits can be seen in Table 3.

Taking into account the spectroscopic orbit by Fletcher (with $a \sin I$ deduced from $K_1 + K_2$, and using the values of $a = 0''1996 \pm 0.0010$ and $I = 117°0 \pm 0.5$ from our orbit), we determine an orbital parallax of $0''02088 \pm 0.0010$ that yields individual masses of $1.70 \pm 0.13\ \mathcal{M}_\odot$ for each component.

We suggest to perform more radial velocity observations with the aim of determining a more robust spectroscopic orbit, which can be used to deduce an orbital parallax closer to the other parallaxes presented in this work. Our parallax gives individual masses of 1.422 and 1.296 $\mathcal{M}_\odot$, which are more in accordance with the spectral types F3V and F6V that we have obtained from the combined spectrum F4V (see Table 1). Gaia did not report a parallax for this binary.

2.2. WDS 09275-5806 (CHR 240, HIP 46388, HD 82082)

The binary nature of this star was discovered by B. Mason in 1996, and it has been followed by A. Tokovinin by means of speckle interferometry in regular observation campaigns since

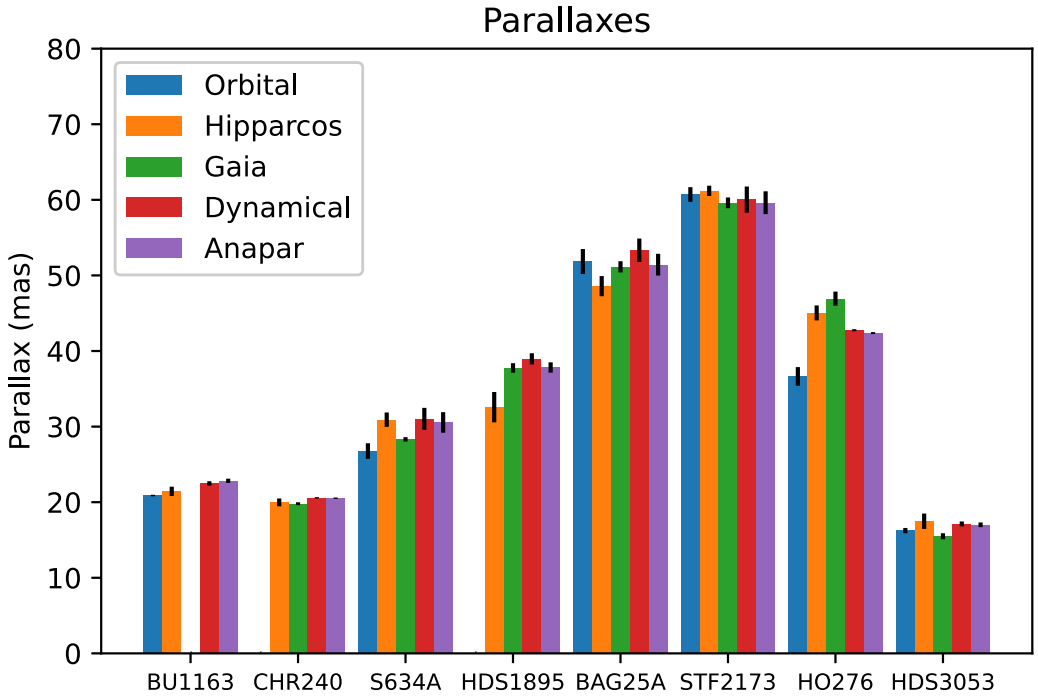

Figure 2. Different parallaxes for each star. They show a good agreement between them in most cases.

2010 (Hartkopf et al. 2012; Tokovinin 2012; Tokovinin et al. 2014, 2015, 2016, 2020).

Despite its very short period (≈1.41 yr), there were only two visual orbits determined by A. Tokovinin (Tokovinin et al. 2015; Tokovinin 2016b), and an astrometric and an astro-spectroscopic orbit reported by Gaia (Gaia Collaboration et al. 2016, 2023). Both of Gaia's orbits are quite similar with respect to the common elements, but there may be an imprecision in the C and H spectroscopic elements, as we will see.

The parallaxes of Hipparcos (0″01997), Gaia (0″01980), and dynamical and ANAPAR (0″02058 and 0″02053) obtained from our orbit, produce mass sums that are in reasonable agreement (between 2.41 and 2.15; see Table 6).

However, when we make an estimation of the parallax using the data from the astro-spectroscopic orbit by Gaia, we obtain values that are not suitable. Be it starting from a combined spectrum of G2V (Houk & Cowley 1975) or G0V (Cannon & Pickering 1993), a Δm of 0.68 (from the speckle measurements) or of 1.2 (from the 6th Catalog of Orbits of Visual Binary Stars (ORB6); Hartkopf et al. 2001a), the individual masses should be within a range of 1.18–1.06 for $\mathcal{M}_A$ and 0.99-0.94 for $\mathcal{M}_B$, and with the value of $a_1 \sin I$ given by Gaia, we reach a linear value of the semimajor axis of the relative orbit, a, within 0″418–0″390. The resulting parallax calculated as $\frac{a''}{a} \approx 0''083$ is very different of the rest of the parallaxes; therefore it suggests that, such as we said earlier, it is quite possible that any of the parameters C, H, or both, have an inadmissible error despite the small uncertainties reported.

2.3. WDS 12114-1647 (S 634 AaAb, HIP 59426, HD 105913)

The A component of the stellar system S 634 (of which three stars were known until recently) is an SB2, which spectroscopic orbit was calculated by Tokovinin (2019) with a period close to seven months (see Table 4). Therefore, in the three-year interval in which A. Tokovinin obtained five speckle measurements at SOAR (resolved for the first time in 2018), the pair AaAb has completed more than five revolutions. The current component B is far from the components AaAb (5″), and for this reason its influence on the close binary is hardly detectable.

Table 5
Parallaxes (in Arcseconds)

WDS Name	Orbital σ	Hipparcos σ	Gaia σ	Dynamical σ	ANAPAR σ
01243-0655	0.02088	0.02144		0.02248	0.02283
BU 1163	0.00010	0.00061		0.00029	0.00028
09275-5806		0.01997	0.01980	0.02058	0.02053
CHR 240		0.00052	0.00019	0.00009	0.00009
12114-1647	0.02676	0.03092	0.02831	0.03103	0.03055
S 634 AaAb	0.00103	0.00095	0.00029	0.00145	0.00136
13317-0219		0.03257	0.03776	0.03896	0.03782
HDS 1895		0.00201	0.00063	0.00074	0.00068
15282-0921	0.05184	0.04858	0.05114	0.05333	0.05142
BAG 25 AaAb	0.00165	0.00133	0.00074	0.00155	0.00144
17304-0104	0.06071	0.06119	0.05960	0.06003	0.05962
STF 2173	0.00097	0.00068	0.00071	0.00173	0.00151
19598-0957	0.03664	0.04504	0.04693	0.04275	0.04237
HO 276	0.00123	0.00099	0.00093	0.00014	0.00013
21274-0701	0.01624	0.01748	0.01549	0.01712	0.01701
HDS 3053	0.00035	0.00102	0.00040	0.00033	0.00031

Note. The different values of the parallaxes expressed in arcseconds figure in this table. The format is the following: once again the first column inform about the identifications of each binary. Columns 2–6 give the values of the different parallaxes (Orbital, Hipparcos, Gaia, Dynamical, and ANAPAR) with their standard errors.

Table 6
The Individual Masses (in $\mathcal{M}_\odot$), With their Standard Errors, Calculated with the Different Parallaxes

WDS Name	Orbital		Hipparcos		Gaia		Dynamical		ANAPAR	
	$\mathcal{M}_A$ σ	$\mathcal{M}_B$ σ	$\mathcal{M}_A$ σ	$\mathcal{M}_B$ σ	$\mathcal{M}_A$ σ	$\mathcal{M}_B$ σ	$\mathcal{M}_A$ σ	$\mathcal{M}_B$ σ	$\mathcal{M}_A$ σ	$\mathcal{M}_B$ σ
01243-0655	1.695	1.695	1.567	1.567			1.422	1.296	1.348	1.249
BU 1163	0.059	0.059	0.143	0.143			0.036	0.033	0.007	0.007
09275-5806			2.108	0.245	2.165	0.249	1.159	0.991	1.151	1.015
CHR 240			0.598	0.569	0.583	0.578	0.009	0.007	0.002	0.002
12114-1647	1.475	1.290	0.956	0.836	1.246	1.090	0.960	0.814	0.990	0.869
S 634 AaAb	0.240	0.210	0.141	0.123	0.148	0.130	0.058	0.049	0.019	0.017
13317-0219			1.873	0.636	1.137	0.473	0.830	0.636	0.886	0.716
HDS 1895			0.487	0.089	0.116	0.036	0.021	0.016	0.007	0.006
15282-0921	0.834	0.574	1.013	0.698	0.869	0.598	0.842	0.451	0.897	0.546
BAG 25 AaAb	0.101	0.070	0.113	0.077	0.075	0.052	0.032	0.017	0.011	0.007
17304-0104	0.971	0.901	0.948	0.880	1.026	0.953	0.973	0.964	0.992	0.985
STF 2173	0.080	0.074	0.071	0.066	0.078	0.072	0.042	0.041	0.011	0.011
19598-0957	1.491	1.507	0.803	0.811	0.710	0.717	1.113	0.775	1.108	0.831
HO 276	0.159	0.160	0.060	0.060	0.049	0.049	0.005	0.003	0.002	0.001
21274-0701	1.763	0.680	1.396	0.538	2.006	0.774	1.172	0.886	1.167	0.933
HDS 3053	0.153	0.059	0.258	0.099	0.195	0.075	0.037	0.028	0.010	0.007

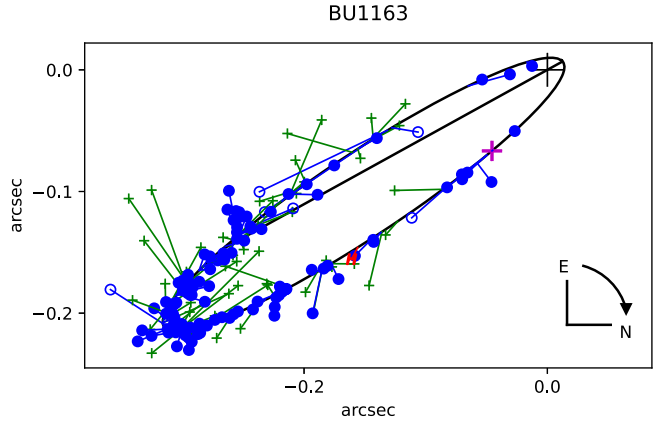

Figure 3. Apparent orbit of BU 1163. The green crosses represent the micrometric observations, the empty blue circles denote observations made with eyepiece interferometer, the red H the Hipparcos observations, the filled blue circles correspond to the speckle observations, and the magenta cross the last observation used in the calculation of the orbit, which provides the current relative position of the components in the apparent orbit.

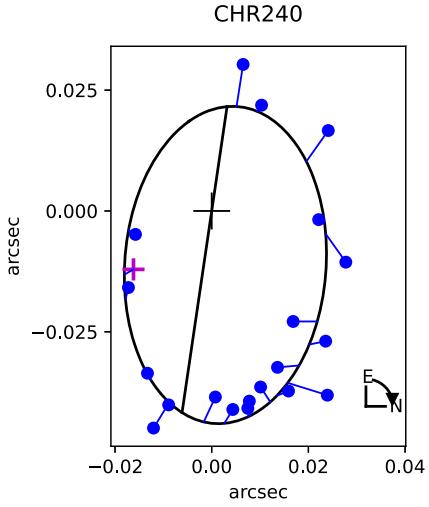

Figure 4. Apparent orbit of CHR 240.

Using these speckle measurements we have determined for the first time (Docobo et al. 2022), and simultaneously to A. Tokovinin (who sent a private communication to ORB6 then unknown to us), the visual orbit with very small rms, both in position angle and angular separation (1.°700 for θ and 0.″0028 for ρ; see Table 3), and also with a good agreement with the common elements of the spectroscopic orbit (see Table 2). We have used the 3D methodology (Docobo et al. 2014) that we already commented in the Introduction with each of the five available observations, and they yield similar orbits with low residuals for the rest of the observations, proving that they are compatible.

With these conditions, from the spectroscopic values of $a_1 \sin I$ and $a_2 \sin I$, and the inclination and the semimajor axis of our orbit, it is possible to deduce the value of the orbital parallax

$$\pi_{\rm Orb} = \frac{a''}{a \text{ (in au)}} = 0''02676 \pm 0''00103. \quad (1)$$

This value is slightly lower than the Gaia parallax ($\pi_{\rm Gaia} = 0''02831 \pm 0.00029$), and clearly smaller than that of Hipparcos ($\pi_{\rm Hip} = 0''03092 \pm 0''00095$), ANAPAR ($\pi_{\rm Ana} = 0''03055 \pm 0.00136$), and dynamical ($\pi_{\rm Dyn} = 0''03103 \pm 0.00145$), see Table 5. This suggests a slight incompatibility between the visual and the spectroscopic orbits, and would merit a monitoring of this system.

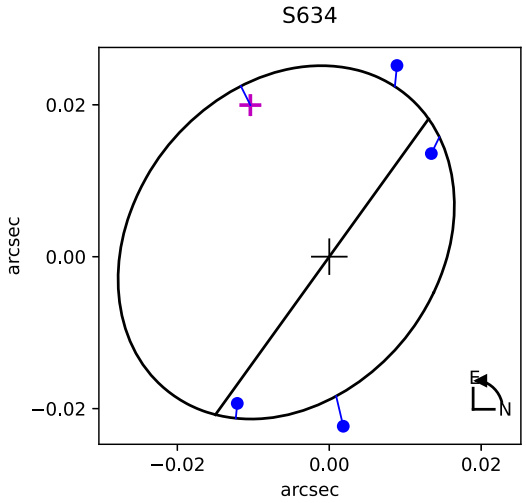

Figure 5. Apparent orbit of S 634 AaAb. .

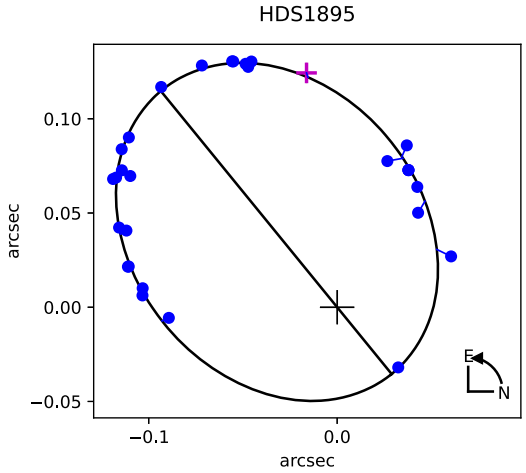

Figure 6. Apparent orbit of HDS 1895.

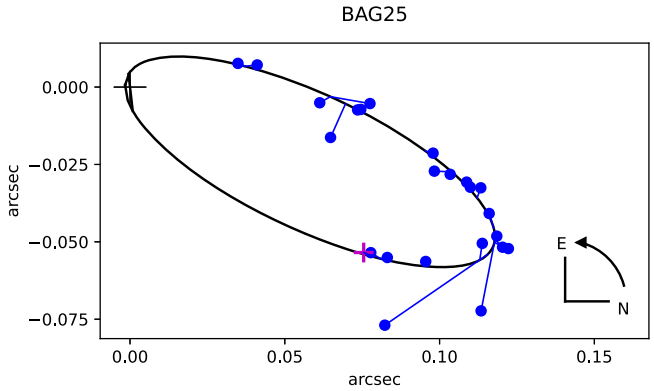

Figure 7. Apparent orbit of BAG 25 AaAb.

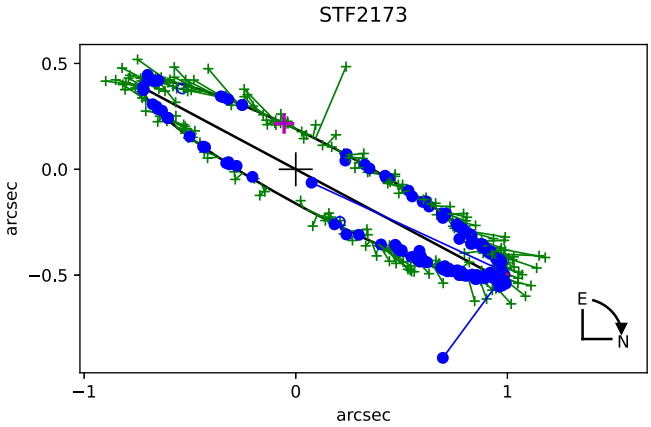

Figure 8. Apparent orbit of STF 2173.

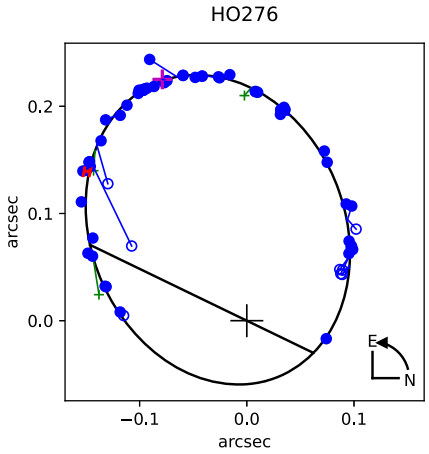

Figure 9. Apparent orbit of HO 276.

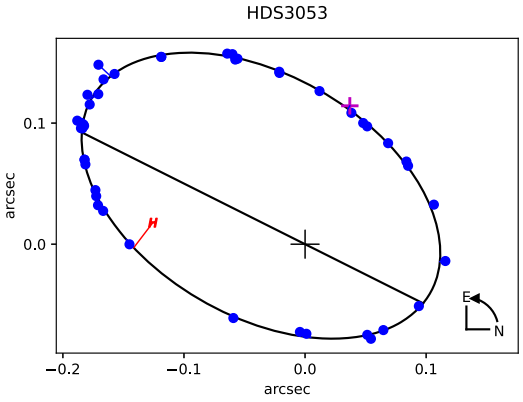

Figure 10. Apparent orbit of HDS 3053.

With respect to the masses calculated for each parallax, they are all very similar (see Table 6), and they are well matched to the spectral types of the components, G3V-G9V, which have been obtained from the combined spectrum G6V and $\Delta m = 0.72$, which was deduced from the speckle registries.

There is also available an astro-spectroscopic solution by Gaia (Gaia Collaboration et al. 2016, 2023), with a slightly larger period (0.581 yr). However their orbital elements do not agree with our solution, especially the angles I, Ω, and ω (see Table 2).

Recently a fourth companion has been detected in the system (R. A. Méndez 2023, private communication). First, it would be necessary to confirm that this new star is physically associated to the system. If so, depending on the separation to the couple AaAb, the perturbations produced by this new component might need to be considered in the dynamics of the close binary.

2.4. WDS 13317-0219 (HDS 1895, HIP 65982, HD 117635)

This star is an SB1, for which the orbit has a period of 1188 days (Latham et al. 2002). As a visual binary it was resolved by means of speckle interferometry from 2001, and several orbits exist as a result of those observations (Hartkopf et al. 2012; Horch et al. 2012; Ren & Fu 2013; Tokovinin et al. 2020; Videla et al. 2022). Some of these visual orbits take as fixed the common elements of the spectroscopic orbit.

Our spectral decomposition yields spectral types of G5.5V + K3V, therefore the expected masses are $\approx 0.9 + 0.7\mathcal{M}_\odot$. The parallax calculated using the ANAPAR methodology matches the one given by Gaia, and using the first, the obtained individual masses are $0.886 + 0.716\mathcal{M}_\odot$. On the other hand, with our orbit and said parallaxes we got a total mass of $\mathcal{M}_1 + \mathcal{M}_2 = 1.61\mathcal{M}_\odot$, which is in good agreement with the previous result. Now, by using the mass function of the spectroscopic orbit $f(\mathcal{M}) = 0.00177297$, and our orbital inclination 20°39:

$$\frac{\mathcal{M}_2^3}{(\mathcal{M}_1 + \mathcal{M}_2)^2} = \frac{f(\mathcal{M})}{\sin^3 I} = 0.042. \quad (2)$$

However, with the values of the masses previously obtained we get:

$$\frac{\mathcal{M}_2^3}{(\mathcal{M}_1 + \mathcal{M}_2)^2} = 0.143. \quad (3)$$

In order to match both values we need to lower the orbital inclination, but in this case the rms in ρ increases. It is also remarkable that the visual orbits with better rms, both in θ and in ρ, have eccentricities lower than 0.55, whereas in the spectroscopic orbit it is 0.64.

2.5. WDS 15282-0921 (BAG 25 AaAb, HIP 75718, HD 137763)

The radial velocities of this SB2 began to be obtained in 1978, although the first SB1 spectroscopic orbit was calculated 13 yr later (Tokovinin 1991). One year later an SB2 orbit appeared (Duquennoy et al. 1992), which was recalculated much later (Halbwachs et al. 2018), although the period was very similar in the three orbits, close to 2.436 yr.

This binary was resolved in 2001 with the 6 m telescope at SAO (Balega et al. 2006b), and it was followed with speckle interferometry mainly by Horch et al. (2012, 2015, 2017) and Tokovinin et al. (2015, 2016, 2020).

A first visual orbit calculated by Jancart et al. (2005) shows positive residuals in ρ for the 23 available observations, which was later corrected (Tokovinin 2016b). Our solution, obtained by applying the 3D methodology (Docobo et al. 2014) improves the rms, and at the same time it breaks the systematic trend of the residuals in theta of the previous orbit. The application of said algorithm shows the coherence among most of the observations of this binary, and supplies a robust solution.

By using the Gaia parallax (see Table 5), our orbit yields a total mass $\mathcal{M}_1 + \mathcal{M}_2 = 1.465 \pm 0.124\mathcal{M}_\odot$, and the mass ratio from the spectroscopic solutions are, $\frac{\mathcal{M}_1}{\mathcal{M}_2} = 1.452 \pm 0.122$ (using the Halbwachs et al. 2018 orbit) and $\frac{\mathcal{M}_1}{\mathcal{M}_2} = 1.494 \pm 0.031$ (using the Duquennoy et al. 1992 orbit). Therefore we can deduce the values of the individual masses:

$$\mathcal{M}_1 = 0.867 \pm 0.085 \quad (4)$$

$$\mathcal{M}_2 = 0.597 \pm 0.059 \quad (5)$$

in the first case, and:

$$\mathcal{M}_1 = 0.878 \pm 0.075 \quad (6)$$

$$\mathcal{M}_2 = 0.587 \pm 0.050. \quad (7)$$

We have decomposed the combined spectrum, G9V, in G8V +M0V. The masses obtained for the primary are a little below that corresponding to the spectral type G8V. In the case of the secondary component, it fits well the typical mass of a M0V spectral type.

2.6. WDS 17304-0104 (STF 2173, HIP 85667, HD 158614)

Since this binary was discovered by W. Struve in 1830 (Aitken & Doolittle 1932), considering a period of around 46 yr, it has completed more than four revolutions, which together with its brightness, and its maximum angular separation of over one arcsecond, has made it a pair with a large number of visual observations in the last 200 yr, including more than 40 of speckle monitoring.

That is why numerous orbits have been calculated, both as a visual (Flammarion 1878; Lewitzky 1896; See 1896; Lewis 1906; Doberck 1910; Aitken 1914; Lohse, included in Aitken & Doolittle 1932; Duncombe & Ashbrook 1952; Starikova 1976; Wilson 1976; Heintz 1994; Söderhjelm 1999; Pourbaix 2000), and as spectroscopic SB2 (Batten et al. 1971, 1991; Duquennoy & Mayor 1991; Pourbaix 2000). In fact, Pourbaix solution takes into account simultaneously both (θ, ρ), and the radial velocities for its determination. The orbit proposed in this paper shows the best rms of all, both in θ and in ρ.

This binary is included in the emblematic catalogs of measurements of Burham (1906), with the number 8083, and Aitken & Doolittle (1932), with the number 10598. In the last one, Aitken says that "The parallax is well determined. The trigonometric value is +0″052 (Yale), the spectroscopic. 0″063 (Mt W) or 0″062 (DAO), the dynamic, 0″066 (J & F) or 0″063 (R & M)."

The spectral type of this binary was listed mainly as a G8IV-V, however it appears as G5V (Sharma et al. 2020) or G6V (Houk & Swift 1999) in the last publications. In the first of these two cases, the decomposition yields G4.5V+G5V, whereas in the second it gives G6V+G6V, as the magnitude difference between the components is only 0.04 (6.06–6.10). In this way, the expected total mass is 1.96 or 1.94 $\mathcal{M}_\odot$, respectively.

Gaia lists the parallaxes of both components: 0″05850 and 0″06071, of which the mean value is 0"05960. Considering our orbital solution, the spectral types G4.5V+G5V, and using the Hipparcos and Gaia parallaxes, as well as the dynamical and ANAPAR parallaxes, we get the results shown in Table 6.

As for the spectroscopic orbits, and taking into account the inclination of 99° from our orbit, the solution of Batten et al. (1991) assigns the largest mass to the secondary component ($0.905 + 1.033\ \mathcal{M}_\odot$), whereas the orbit by Batten et al. (1971) yields a total mass of 2.145 $\mathcal{M}_\odot$. The other two orbits (Duquennoy & Mayor 1991; Pourbaix 2000) lead to total masses slightly lower than 2 $\mathcal{M}_\odot$.

With respect to the orbital parallaxes, and making use of the value of $a \sin I$ from each of the spectroscopic orbits, and the

value of the semimajor axis (a'') and the inclination of our orbit, the following values are deduced:

1. 0″06071 (with the Pourbaix orbit).
2. 0″06002 (Batten et al. orbit).
3. 0″05987 (Duquennoy & Mayor orbit).
4. 0″05803 (Batten, Fletcher & West orbit).

As we can see, all the parallaxes for this binary are in good agreement.

This binary shows a large proper motion. According to the data from Hipparcos (Perryman et al. 1997; van Leeuwen 2007): (−127.77, −168.61) mas yr^{-1}. Gaia, for its part (Gaia Collaboration et al. 2016, 2018), gives separate values for each component: (−138.31155679907, −144.41982410308927) mas yr^{-1}, and (−120.59892576351368, -208.53898150434344) mas yr^{-1}, which are affected by the orbital motion.

2.7. WDS 19598-0957 (HO 276, HIP 98416, HD 189340)

Burnham (1906) points in his catalog of measurements that in 1887 G. W. Hough described this star as elongated, but he was not able to resolve it, as it was not possible either in 1890 by the same S. W. Burnham, between 1903 and 1906 by E. Doolittle, and in 1906 by R. G. Aitken (Burnham 1906). It was Finsen (1962) the first to obtain the position angle and the separation of this short-period binary (less than 5 yr). Burnham also alerted of its notable proper motion. The Gaia DR2 (Gaia Collaboration et al. 2016, 2018) following values for the proper motion are listed as: −272.764 and −404.804.

The first orbit was announced by Baize (1990, 1992), as circular and with a period of 9.7 yr. However, Duquennoy & Mayor (1991) obtained almost simultaneously SB1 and SB2 solutions with periods 4.649 and 4.901 yr, respectively, showing that the orbital period really was half of that determined by Baize (1990, 1992) and that the orbital eccentricity was close to 0.6. Despite this fact, in the following years long-period low-eccentricity orbits were determined (Hartkopf et al. 1996; Söderhjelm 1999).

Pourbaix (2000) calculated a solution fitting both the visual measurements and the radial velocities. Such an orbit showed almost from the publication years systematically positive residuals in the position angle, probably because the radial velocities do not cover strategical parts of the orbit, and that is why it was revised by Tokovinin (2017). The orbit presented in this paper clearly improves the rms of all the previous orbits.

The mean of the magnitude differences between the components from the speckle measurements is 1.59, which is coherent with the visual magnitudes from Hipparcos, 6.22 and 7.83, given in the WDS catalog. With respect to the combined spectrum, according to the different measurements gathered in Simbad (Roman 1955; Eggen 1962; Malaroda 1975; Cannon & Pickering 1993; Houk & Swift 1999; Gray et al. 2003), it is between F8 and G2. For example, with F9V (Gray et al. 2003) and the speckle magnitude difference, F6V and G8V are deduced, whereas with G2V (Houk & Swift 1999) the decomposition yields F9.5V and K1V. In the first case the standard masses would be $1.25 + 0.94 = 2.19\mathcal{M}_{\odot}$, and in the second $1.08 + 0.86 = 1.94\mathcal{M}_{\odot}$.

Table 6 shows the values of the masses obtained from the different parallaxes.

As for the orbital parallax, and also the masses derived, should be the most precise, but for it to be true both orbits (visual and spectroscopic) have to be of the best quality, which is not this case. The spectroscopic orbit must be improved by filling the whole orbital phase with radial velocities because currently there are strategic areas that are not well covered, mainly close to the maximal and the minimal value of the radial velocity.

2.8. WDS 21274-0701 (HDS 3053, HIP 105947, HD 204236)

This is a hierarchical triple system composed by a binary, for which the main component is in turn an SB1 (Tokovinin 2018b). The initial binary, components A and B, was discovered by Hipparcos (Perryman et al. 1997), whereas Nordström et al. (2004), by studying the radial velocities of the system, detected the spectroscopic subcomponent, AaAb, for which the orbital period is 8.7279 days (see Table 4).

Several orbits have been calculated (Balega et al. 2006a; Mason et al. 2010; Tokovinin et al. 2015; Tokovinin 2018b; Mitrofanova et al. 2021) from the speckle observations, which were performed mainly by Balega et al. (2002, 2006, 2007, 2013), Tokovinin et al. (2010a, 2010b, 2014, 2015, 2016), and Mitrofanova et al. (2021), and occasionally by Mason et al. (1999, 2010) and Horch et al. (2008, 2009, 2011). Also, Tokovinin (2018b) completed his visual solution with SB2 elements by using three radial velocity measurements, and at the same time, he determined the position of the ascending node. Moreover, the orbit as an SB1 of Ab around Aa was published in the same article.

From visual magnitudes 7.97 and 9.14 for the A and B components, and a combined spectral type of G0V, its decomposition yields F8.5V and G8V for AaAb and B, respectively. If we now separate the spectral type F8.5V of AaAb as a function of the magnitude difference, Δm, we get the results shown in Table 7, in which we have assumed a mass of 0.94 for component B (spectral type G8V).

On the other hand, by using the values of a'' and the inclination of the orbit of B with respect to AaAb, along with $a \sin I$ from the SB2 orbit, it is deduced an orbital parallax of:

$$\pi_{\rm Orb} = \frac{a''}{a\ (\text{in au})} = 0''01617, \tag{8}$$

which, when inserted in the expression,

$$\mathcal{M}_{Aa} + \mathcal{M}_{Ab} + \mathcal{M}_{B} = \frac{\left(\frac{a''}{\pi_{\rm Orb}}\right)^3}{P^2}, \tag{9}$$

yields the value of the total mass of the triple system, 2.443 $\mathcal{M}_{\odot}$, which is close to the value of $\Delta m = 7$ of Table 7. With these individual masses, the mass function, $f(\mathcal{M}) = 0.0184921$, of this orbit yields an inclination of $I_{12} = 70°$. Here we have used the subscript 12 to denote orbit of Ab with respect to Aa. However, if we consider the Gaia DR3 parallax, 0″01549, slightly lower than the orbital parallax, Equation (9) gives a total mass of 2.80 $\mathcal{M}_{\odot}$, which is close to the case of $\Delta m = 4.5$, with masses $\mathcal{M}_{Aa} = 1.23$ (Sp. F6.5V), and $\mathcal{M}_{Ab} = 0.63$, and an orbital inclination $I_{12} = 39°5$.

Table 7
Spectral Decomposition of HDS 3053 According To The Magnitude Difference of AaAb

Δm	Spectral type Aa	Spectral type Ab	Mass Aa ($\mathcal{M}_\odot$)	Mass Ab ($\mathcal{M}_\odot$)	Mass B ($\mathcal{M}_\odot$)	Total mass ($\mathcal{M}_\odot$)
1	F6V	G1.5V	1.25	1.05	0.94	3.20
2	F5.5V	G9V	1.29	0.90	0.94	3.13
3	F5.5V	K3V	1.29	0.78	0.94	3.01
4	F6V	K6V	1.25	0.69	0.94	2.88
5	F7V	M0V	1.21	0.57	0.94	2.72
6	F8V	M2V	1.18	0.44	0.94	2.56
7	F8.5V	M3V	1.15	0.37	0.94	2.46

Note. Column 1 contains the magnitude difference, with a step of 1 magnitude; columns 2 and 3 show the spectral types of the components Aa and Ab, respectively, calculated from Δm; columns 4 and 5 the corresponding calibrated masses; column 6 yields the mass of the component B; and column 7 the total mass. All masses are given in units of solar mass.

Table 8
Absolute Magnitudes And luminosities Obtained from the ANAPAR Parallax

Star	M_{VA}	M_{VB}	L_A ($L_\odot$)	L_B ($L_\odot$)
BU1163	3.32	3.71	3.79± 0.21	2.67± 0.15
CHR 240	4.14	4.82	1.82± 0.04	1.01± 0.02
S 634 AaAb	4.91	5.63	0.93± 0.19	0.51± 0.11
HDS 1895	5.49	6.81	0.58± 0.05	0.23± 0.02
BAG 25 AaAb	5.45	8.94	0.60± 0.08	0.06± 0.01
STF 2173	4.91	4.95	0.94± 0.11	0.91± 0.11
HO 276	4.32	5.93	1.56± 0.02	0.41± 0.01
HDS 3053	4.03	5.20	1.99± 0.17	0.73± 0.06

Table 9
Temperature and Metallicity

WDS Hipparcos	Name	Metalicity	Catalogue (year)	log ($T_{\rm eff}$)	$v/v_{\rm crit}$
01243-0655	BU 1163	−0.15	Gaspar+ (2016)	3.832 3.832	0.0
09275-5806	CHR 240	0.11	Holmberg+ (2009)	3.774 3.745	0.0
12114-1647	S 634 AaAb	0.02	Holmberg+ (2009)	3.757 3.718	0.0
13317-0219	HDS 1895	−0.33	Soubiran+ (2016)	3.748 3.671	0.0
15282-0921	BAG 25 AaAb	0.09	Soubiran+ (2016)	3.725 3.584	0.0
17304-0104	STF 2173	0.01	Soubiran+ (2016)	3.748 3.744	0.0
19598-0957	HO 276	−0.06	Soubiran+ (2016)	3.779 3.698	0.0
21274-0701	HDS 3053	0.02	Holmberg+ (2009)	3.791 3.725	0.0

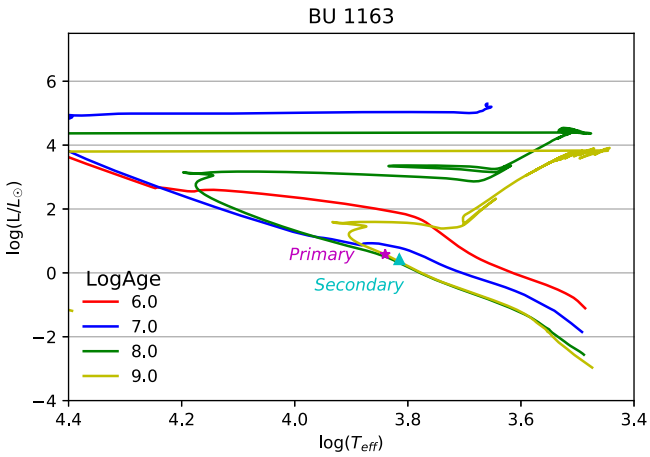

Figure 11. HR diagram and isochrones for BU 1163.

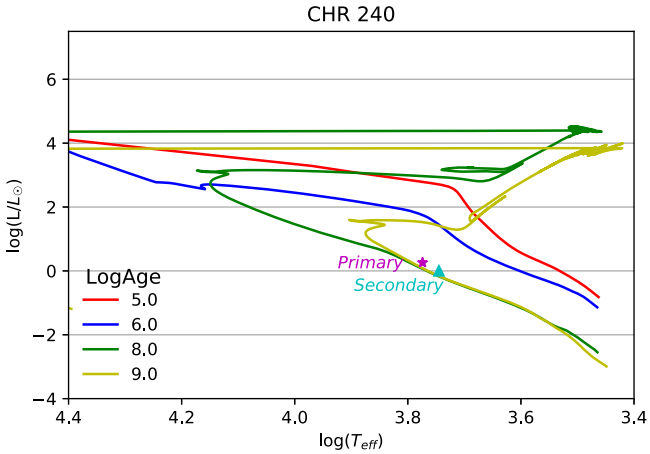

Figure 12. HR diagram and isochrones for CHR 240.

3. Luminosities and Ages

In order to calculate the luminosities with the expression (Torres 2010):

$$\log \frac{L}{L_\odot} = -0.4(M_V - V_\odot - 31.572 + (BC_V - BC_\odot)). \quad (10)$$

The value of $V_\odot$ was adopted from Torres (2010) and the bolometric corrections adopted from Pecaut & Mamajek (2013)

As usual, $L_\odot$ and $V_\odot$ are the luminosity and the apparent visual magnitude of the Sun, BC_V and $BC_\odot$ are, respectively, the bolometric corrections of the star and the Sun in the V band, and M_V is the absolute V magnitude of the star.

To obtain the M_V of the components, the apparent V magnitudes were corrected by the interstellar extinction, A_V, using the Parenago formula, depending on the distance, d, and the galactic latitude, b, as described in Malkov et al. (2018):

$$A_V = \frac{a_0 \beta}{\sin|b|}(1 - e^{\frac{-d \sin|b|}{\beta}}) \quad (11)$$

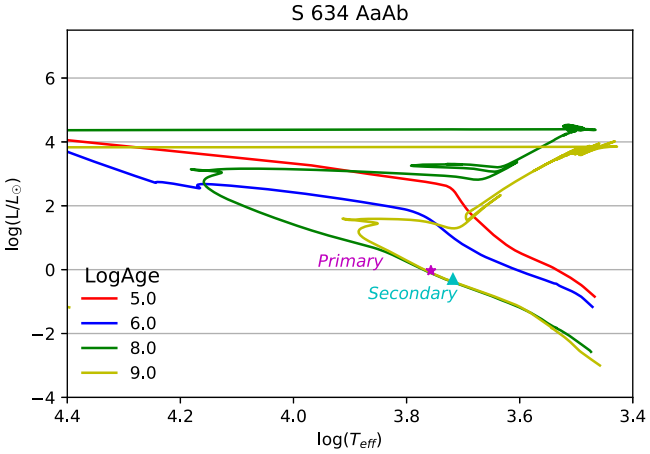

Figure 13. HR diagram and isochrones for S 634 AaAb.

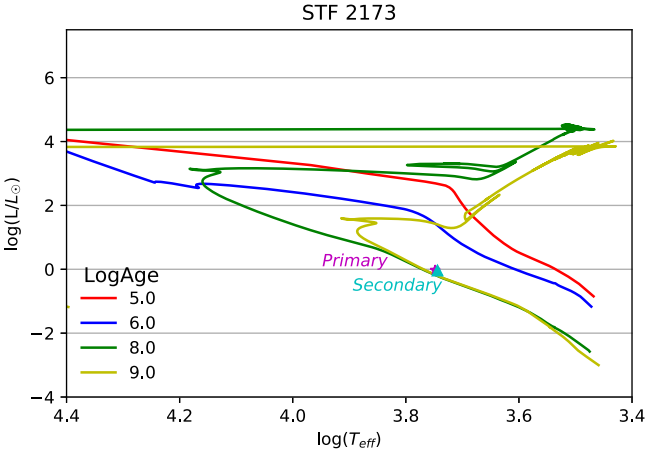

Figure 16. HR diagram and isochrones for STF 2173.

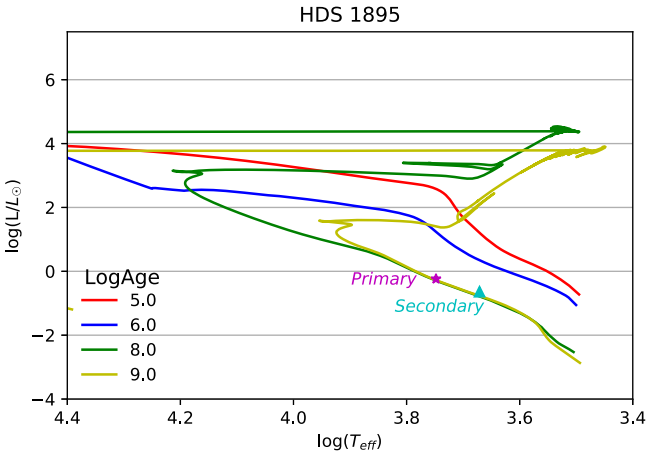

Figure 14. HR diagram and isochrones for HDS 1895.

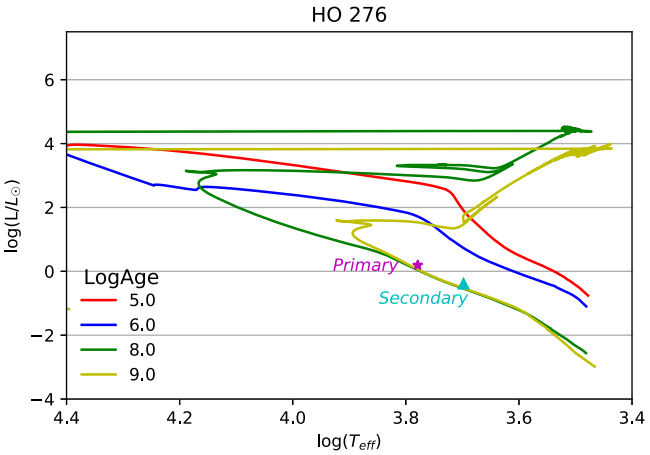

Figure 17. HR diagram and isochrones for HO 276.

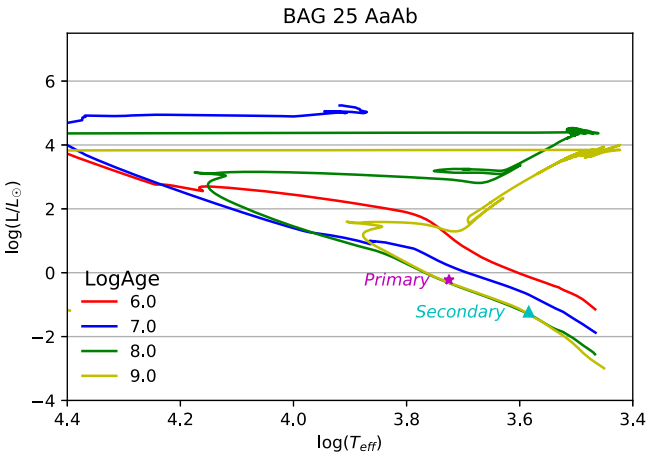

Figure 15. HR diagram and isochrones for BAG 25 AaAb.

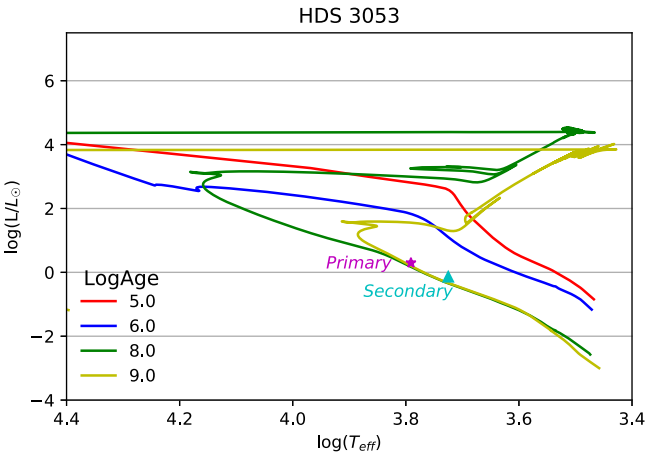

Figure 18. HR diagram and isochrones for HDS 3053.

where a_0 is the absorption per kpc and β is the vertical scale of the absorbing matter distribution, with an estimated value of 1.6 mag kpc^{-1} and 114 pc, respectively (Sharov 1964). After the extinction was applied, the ANAPAR parallaxes, shown in the Table 8, were used.

Table 8 shows the name of the star in the first column, the calculated M_V of the components appear in the second and third columns, and the luminosities are shown in the fourth and fifth columns.

To obtain information associated with system ages, we used their metallicity values from Holmberg et al. (2009), Gáspár et al. (2016), and Soubiran et al. (2016). We applied the relations between the spectral type and effective temperature given by de Jager & Nieuwenhuijzen (1987). The isochrones were provided by MIST version 1.2 (Paxton et al. 2011,

2013, 2015; Choi et al. 2016; Dotter 2016; Paxton et al. 2018). According to their masses, we set initial $v/v_{\rm crit} = 0.0$ for all the systems. The values utilized to calculate the isochrones can be seen in Table 9.

We plotted the pair (Teff, $\log \frac{L}{L_\odot}$) of the primary and secondary components of the systems in HR diagrams (see Figures 11–18) showing the isochrones of the most probable ages of the system. The data do not support a definitive value for some system ages. However, we can see that the calculated luminosities are consistent with system coevolution indicating that both components have the same origin.

4. Conclusions

Once again, the HRCam attached to the 4.1 m SOAR telescope confirms the suitability of this instrumentation + telescope to continue performing speckle observations in the future, especially of austral close binaries.

In the present research, using this class of measurements obtained since 2019–2022, the authors have been able to improve the visual orbits of eight binaries taking into account that each of these binaries has also an spectroscopic orbit. So, in these conditions the information achieved is maximum both regarding the different parallaxes: orbital, dynamical, ANA-PAR, and those corresponding to the Hipparcos and Gaia missions, and on the other hand concerning the values of the masses derived from the parallaxes. In all of the cases, individual masses have been reported.

It is important to recommend also the improving of some of the spectroscopic orbits involved in the present work. RV velocities close to strategic points of the orbits are necessary in order to determine orbital parallaxes with high quality.

In addition to this, using absolute luminosities with data regarding the metallicities and effective temperatures, the position of the sixteen components in the HR diagram against the most suitable isochrones produced by MIST has been plotted. All of these plots show similar ages for the components and are coherent with a coevolution and common origin context.

This is the fourth paper on binaries produced by the collaboration between the University of Chile and the University of Santiago de Compostela (Galicia, Spain).

Acknowledgments

This paper is based on observations obtained at the Southern Astrophysical Research Observatory (SOAR) telescope, which is a joint project of the Ministério da Ciência, Tecnologia, e Inovaçao (MCTI) da Republica Federativa do Brasil, the U.S. National Optical Astronomy Observatory (NOAO), the University of North Carolina at Chapel Hill (UNC), and Michigan State University (MSU).

We are very grateful for the continuous support of the Chilean Telescope Allocation Committee: http://www.das.uchile.cl/das_cntac.html under programs CN2018A-1, CN2019A-2, CN2019B-13, CN2020A-19, CN2020B-10, CN2021B-17, CN2022A-11, CN2022B-14, and CN2023A-7 for SOAR.

During this research, the authors used the SIMBAD service operated by the Centre des Données Stellaires (Strasbourg, France; Wenger et al. 2000); bibliographic references from the Astrophysics Data System maintained by SAO/NASA; the Site Informatique des étoiles Doubles de Nice (SIDONIe; Le Contel et al. 2001) compiled principally by Dr. Paul Couteau; the historical database of micrometric measurements provided by the WDS (Mason et al. 2001b) the Catalogue of Interferometric Measurements of Binary Stars (WDS INT4; Hartkopf et al. 2001b); and the Sixth Catalogue of Orbits of Visual Binary Stars (WDS ORB6; Hartkopf et al. 2001a), all of them maintained at USNO.

This work has used data from the European Space Agency (ESA) mission Gaia (https://www.cosmos.esa.int/gaia), processed by the Gaia Data Processing and Analysis Consortium (DPAC,https://www.cosmos.esa.int/web/gaia/dpac/consortium). Funding for the DPAC has been provided by national institutions, in particular, the institutions participating in the Gaia Multilateral Agreement.

The authors thank Andrei Tokovinin for his collaboration with speckle runs carried out at SOAR in 2019, 2020, 2021, and 2022. R.A.M. and E.C. thank the funding from the Vicerrectoría de Investigación y Desarrollo (VID) of the Universidad de Chile, project: ENL02/23.

This paper was supported by the Spanish Ministerio de Ciencia e Innovación under the Project PID2021-122608NB-I00 (AEI/FEDER, UE).

Facility: SOAR.

ORCID iDs

José A. Docobo https://orcid.org/0000-0001-9556-8624
Pedro P. Campo https://orcid.org/0000-0001-7268-5879
Jorge Gómez https://orcid.org/0000-0003-0397-951X
René A. Méndez https://orcid.org/0000-0003-1454-0596
Edgardo Costa https://orcid.org/0000-0003-4142-1082

References

Abt, H. A. 2009, ApJS, 180, 117
Aitken, R. G. 1914, PLicO, 12, 1
Aitken, R. G., & Doolittle, E. 1932, New General Catalogue of Double Stars within 120 of the North Pole
Al-Shukri, A. M., McAlister, H. A., Hartkopf, W. I., Hutter, D. J., & Franz, O. G. 1996, AJ, 111, 393
Andrade, M. 2019, A&A, 630, A96
Anguita-Aguero, J., Mendez, R. A., Clavería, R. M., & Costa, E. 2022, AJ, 163, 118
Baize, P. 1990, IAUDS, 112, 1
Baize, P. 1992, A&AS, 92, 31
Baize, P., & Romani, L. 1946, AnAp, 9, 13
Balega, I., Bonneau, D., & Foy, R. 1984, A&AS, 57, 31
Balega, I. I., Balega, Y. Y., Hofmann, K.-H., et al. 2002, A&A, 385, 87
Balega, I. I., Balega, Y. Y., Hofmann, K. H., et al. 2006a, A&A, 448, 703
Balega, I. I., Balega, Y. Y., Maksimov, A. F., et al. 2006b, BSAO, 59, 20
Balega, I. I., Balega, Yu. Yu., Maksimov, A. F., et al. 2007, AstBu, 62, 339
Balega, I. I., Balega, Yu. Yu., Gasanova, L. T., et al. 2013, AstBu, 68, 53
Barlow, D. J., Fekel, F. C., & Scarfe, C. D. 1993, PASP, 105, 476
Batten, A. H., Fletcher, J. M., Hill, G., Lu, W., & Morbey, C. L. 1991, PASP, 103, 294
Batten, A. H., Fletcher, J. M., & West, F. R. 1971, PASP, 83, 149
Branham, R. L. 2005, ApJ, 622, 613
Burnham, S. W. 1906, A General Catalogue of Double Stars within 121 of the North Pole (Chicago, IL: Univ. Chicago Press)
Campo, P. P. 2019, Phd thesis, Univ. Santiago de Compostela, http://hdl.handle.net/10347/20490
Cannon, A. J., & Pickering, E. C. 1993, yCat, III/135A
Catovic, Z., & Olevic, D. 1992, in ASP Conf. Ser. 32, IAU Coll. 135: Complementary Approaches to Double and Multiple Star Research, ed. H. A. McAlister & W. I. Hartkopf (San Francisco, CA: ASP), 217
Choi, J., Dotter, A., Conroy, C., et al. 2016, ApJ, 823, 102
Cid, R. 1958, AJ, 63, 395
Cid, R. 1960, RvACZ, 15, 37
Davidson, J. W. J., Baptista, B. J., Horch, E. P., Franz, O., & van Altena, W. F. 2009, AJ, 138, 1354

de Jager, C., & Nieuwenhuijzen, H. 1987, A&A, 177, 217
Doberck, W. 1910, AN, 184, 131
Docobo, J. A. 1985, CeMec, 36, 143
Docobo, J. A. 2012, in Orbital Couples: Pas de Deux in the Solar System and the Milky Way, ed. F. Arenou & D. Hestroffer (Paris: Paris Observatory), 119
Docobo, J. A., Campo, P. P., Andrade, M., & Horch, E. P. 2014, AstBu, 69, 461
Docobo, J. A., Campo, P. P., Méndez, R. A., & Costa, E. 2022, IAUDS, 207, 1
Docobo, J. A., Campo, P. P., Méndez, R. A., & Costa, E. 2023, IAUDS, 209, 1
Docobo, J. A., & Ling, J. F. 2003, A&A, 409, 989
Dotter, A. 2016, ApJS, 222, 8
Douglass, G. G., Mason, B. D., Rafferty, T. J., Holdenried, E. R., & Germain, M. E. 2000, AJ, 119, 3071
Duncombe, R. L., & Ashbrook, J. 1952, AJ, 57, 92
Duquennoy, A., & Mayor, M. 1991, A&A, 248, 485
Duquennoy, A., Mayor, M., Andersen, J., Carquillat, J. M., & North, P. 1992, A&A, 254, L13
Edwards, T. W. 1976, AJ, 81, 245
Eggen, O. J. 1962, RGOB, 51, 79
Evans, D. S. 1957, MNSSJ, 16, 20
Finsen, W. S. 1962, ROCi, 121, 10
Finsen, W. S. 1973, Circ. d'Inf., 61, 1
Flammarion, C. 1878, Catalogue des étoiles doubles et multiples en mouvement relatif certain, comprenant toutes les observations faites sur chaque couple depuis sa découverte, et les résultats conclus de l'étude des mouve (Paris: Gauthier-Villars)
Fletcher, J. M. 1973, JRASC, 67, 255
Frasca, A., Covino, E., Spezzi, L., et al. 2009, A&A, 508, 1313
Fu, H. H., Hartkopf, W. I., Mason, B. D., et al. 1997, AJ, 114, 1623
Gaia Collaboration, Brown, A. G. A., Vallenari, A., et al. 2018, A&A, 616, A1
Gaia Collaboration, Prusti, T., de Bruijne, J. H. J., et al. 2016, A&A, 595, A1
Gaia Collaboration, Vallenari, A., Brown, A. G. A., et al. 2023, A&A, 674, A1
Gáspár, A., Rieke, G. H., & Ballering, N. 2016, ApJ, 826, 171
Gray, R. O., Corbally, C. J., Garrison, R. F., et al. 2006, AJ, 132, 161
Gray, R. O., Corbally, C. J., Garrison, R. F., McFadden, M. T., & Robinson, P. E. 2003, AJ, 126, 2048
Halbwachs, J. L., Mayor, M., & Udry, S. 2018, A&A, 619, A81
Hartkopf, W. I., Mason, B. D., Barry, D. J., et al. 1993, AJ, 106, 352
Hartkopf, W. I., Mason, B. D., & McAlister, H. A. 1996, AJ, 111, 370
Hartkopf, W. I., Mason, B. D., McAlister, H. A., et al. 2000, AJ, 119, 3084
Hartkopf, W. I., Mason, B. D., & Worley, C. E. 2001a, AJ, 122, 3472
Hartkopf, W. I., McAlister, H. A., & Franz, O. G. 1989, AJ, 98, 1014
Hartkopf, W. I., McAlister, H. A., & Franz, O. G. 1992, AJ, 104, 810
Hartkopf, W. I., McAlister, H. A., Mason, B. D., et al. 1997, AJ, 114, 1639
Hartkopf, W. I., McAlister, H. A., & Mason, B. D. 2001b, AJ, 122, 3480
Hartkopf, W. I., Tokovinin, A., & Mason, B. D. 2012, AJ, 143, 42
Heintz, W. D. 1978, Double Stars, Vol. 15 (Dordrecht: D. Reidel)
Heintz, W. D. 1994, AJ, 108, 2338
Holmberg, J., Nordström, B., & Andersen, J. 2009, A&A, 501, 941
Horch, E., Franz, O. G., & Ninkov, Z. 2000, AJ, 120, 2638
Horch, E., Ninkov, Z., & Franz, O. G. 2001a, AJ, 121, 1583
Horch, E., Ninkov, Z., van Altena, W. F., et al. 1999, AJ, 117, 548
Horch, E., van Altena, W. F., Girard, T. M., et al. 2001b, AJ, 121, 1597
Horch, E. P., Bahi, L. A. P., Gaulin, J. R., et al. 2012, AJ, 143, 10
Horch, E. P., Baptista, B. J., Veillette, D. R., & Franz, O. G. 2006a, AJ, 131, 3008
Horch, Elliott P., van Altena, William F., Cyr, William M., et al. 2008, AJ, 136, 312
Horch, Elliott P., Falta, David, Anderson, Lisa M., et al. 2009, AJ, 139, 205
Horch, E. P., Casetti-Dinescu, D. I., Camarata, M. A., et al. 2017, AJ, 153, 212
Horch, E. P., Franz, O. G., & van Altena, W. F. 2006b, AJ, 132, 2478
Horch, E. P., Gomez, S. C., Sherry, W. H., et al. 2011, AJ, 141, 45
Horch, E. P., Meyer, R. D., & van Altena, W. F. 2004, AJ, 127, 1727
Horch, E. P., Robinson, S. E., Meyer, R. D., et al. 2002, AJ, 123, 3442
Horch, E. P., van Belle, G. T., Davidson, J. W. J., et al. 2015, AJ, 150, 151
Houk, N., & Cowley, A. P. 1975, University of Michigan Catalogue of Two-dimensional Spectral Types for the HD Star, Vol. I (Ann Arbor, MI: Univ. Michigan)
Houk, N., & Swift, C. 1999, Michigan Spectral Survey, 5, 0
Ishida, G. 1966, PASP, 78, 273
Jancart, S., Jorissen, A., Babusiaux, C., & Pourbaix, D. 2005, A&A, 442, 365
Labeyrie, A. 1970, A&A, 6, 85
Latham, D. W., Stefanik, R. P., Torres, G., et al. 2002, AJ, 124, 1144
Le Contel, D., Valtier, J. C., & Bonneau, D. 2001, A&A, 377, 496
Lewis, T. 1906, MmRAS, 56, 1
Lewitzky, G. 1896, AN, 139, 285
MacKnight, M., & Horch, E. P. 2004, AAS Meeting Abstracts, 204, 07
Malaroda, S. 1975, AJ, 80, 637
Malkov, O., Karpov, S., Kilpio, E., et al. 2018, OAst, 27, 62
Mason, B. D., Hartkopf, W. I., Gies, D. R., Henry, T. J., & Helsel, J. W. 2009, AJ, 137, 3358
Mason, B. D., Hartkopf, W. I., Holdenried, E. R., & Rafferty, T. J. 2001a, AJ, 121, 3224
Mason, B. D., Hartkopf, W. I., & Tokovinin, A. 2010, AJ, 140, 735
Mason, B. D., Hartkopf, W. I., Urban, S. E., et al. 2002, AJ, 124, 2254
Mason, B. D., Hartkopf, W. I., Wycoff, G. L., et al. 2001b, AJ, 122, 1586
Mason, B. D., Martin, C., Hartkopf, W. I., et al. 1999, AJ, 117, 1890
Mason, B. D., Wycoff, G. L., Hartkopf, W. I., Douglass, G. G., & Worley, C. E. 2001b, AJ, 122, 3466
McAlister, H. A. 1976, PASP, 88, 957
McAlister, H. A. 1977, ApJ, 212, 459
McAlister, H. A. 1978, ApJ, 223, 526
McAlister, H. A., & Degioia, K. A. 1979, ApJ, 228, 493
McAlister, H. A., & Fekel, F. C. 1980, ApJS, 43, 327
McAlister, H. A., & Hartkopf, W. I. 1984, Catalog of Interferometric Measurements of Binary Stars
McAlister, H. A., Hartkopf, W. I., Hutter, D. J., & Franz, O. G. 1987, AJ, 93, 688
McAlister, H. A., & Hendry, E. M. 1982, ApJS, 48, 273
McAlister, H. A., Hendry, E. M., Hartkopf, W. I., Campbell, B. G., & Fekel, F. C. 1983, ApJS, 51, 309
Mendez, R. A., Claveria, R. M., Orchard, M. E., & Silva, J. F. 2017, AJ, 154, 187
Mitrofanova, A., Dyachenko, V., Beskakotov, A., et al. 2021, AJ, 162, 156
Monet, D. G. 1979, ApJ, 234, 275
Morbey, C. L. 1975, PASP, 87, 689
Nordström, B., Mayor, M., Andersen, J., et al. 2004, A&A, 418, 989
Olević, D., & Cvetković, Z. 2004, A&A, 415, 259
Paxton, B., Bildsten, L., Dotter, A., et al. 2011, ApJS, 192, 3
Paxton, B., Cantiello, M., Arras, P., et al. 2013, ApJS, 208, 4
Paxton, B., Marchant, P., Schwab, J., et al. 2015, ApJS, 220, 15
Paxton, B., Schwab, J., Bauer, E. B., et al. 2018, ApJS, 234, 34
Pecaut, M. J., & Mamajek, E. E. 2013, ApJS, 208, 9
Perryman, M. A. C., Lindegren, L., Kovalevsky, J., et al. 1997, A&A, 323, L49
Pourbaix, D. 1998, A&AS, 131, 377
Pourbaix, D. 2000, A&AS, 145, 215
Ren, S., & Fu, Y. 2013, AJ, 145, 81
Roman, N. G. 1955, ApJS, 2, 195
Sebring, T. A., Krabbendam, V. L., & Heathcote, S. R. 2003, Proc. SPIE, 4837, 71
See, T. J. J. 1896, Researches on the Evolution of the Stellar Systems (London: The Nichols Press)
Sharma, K., Kembhavi, A., Kembhavi, A., et al. 2020, MNRAS, 491, 2280
Sharov, A. S. 1964, SvA, 7, 689
Söderhjelm, S. 1999, A&A, 341, 121
Soubiran, C., Le Campion, J. F., Brouillet, N., & Chemin, L. 2016, A&A, 591, A118
Starikova, G. A. 1976, ATsir, 922, 6
Starikova, G. A. 1978, ATsir, 1002, 3
Tokovinin, A. 2012, AJ, 144, 56
Tokovinin, A. 2016a, ORBIT: IDL Software for Visual, Spectroscopic, and Combined Orbits, Zenodo, doi:10.5281/zenodo.61119
Tokovinin, A. 2016b, AJ, 152, 138
Tokovinin, A. 2017, AJ, 154, 110
Tokovinin, A. 2018a, PASP, 130, 035002
Tokovinin, A. 2018b, AJ, 156, 48
Tokovinin, A. 2019, AJ, 158, 222
Tokovinin, A., & Cantarutti, R. 2008, PASP, 120, 170
Tokovinin, A., Cantarutti, R., Tighe, R., et al. 2010a, PASP, 122, 1483
Tokovinin, A., Mason, B. D., & Hartkopf, W. I. 2010b, AJ, 139, 743
Tokovinin, A., Mason, B. D., & Hartkopf, W. I. 2014, AJ, 147, 123
Tokovinin, A., Mason, B. D., Hartkopf, W. I., Mendez, R. A., & Horch, E. P. 2015, AJ, 150, 50
Tokovinin, A., Mason, B. D., Hartkopf, W. I., Mendez, R. A., & Horch, E. P. 2016, AJ, 151, 153
Tokovinin, A., Mason, B. D., Hartkopf, W. I., Mendez, R. A., & Horch, E. P. 2018, AJ, 155, 235
Tokovinin, A., Mason, B. D., Mendez, R. A., et al. 2021, AJ, 162, 41
Tokovinin, A., Mason, B. D., Mendez, R. A., & Costa, E. 2022, AJ, 164, 58

Tokovinin, A., Mason, B. D., Mendez, R. A., Costa, E., & Horch, E. P. 2020, AJ, 160, 7
Tokovinin, A., Mason, B. D., Mendez, R. A., Horch, E. P., & Briceño, C. 2019, AJ, 158, 48
Tokovinin, A. A. 1982, SvAL, 8, 22
Tokovinin, A. A. 1983, SvAL, 9, 293
Tokovinin, A. A. 1985, A&AS, 61, 483
Tokovinin, A. A. 1991, A&AS, 91, 497
Tokovinin, A. A., & Ismailov, R. M. 1988, A&AS, 72, 563
Torres, G. 2010, AJ, 140, 1158
van den Bos, W. H. 1934, CiUO, 92, 105
van den Bos, W. H. 1956, MNSSJ, 15, 39
van den Bos, W. H. 1962, PASP, 74, 291
van Leeuwen, F. 2007, A&A, 474, 653
Vidal, E. 1953, Cálculo de órbitas de estrellas dobles visuales (Santiago de Compostela: Consejo Superior de Investigaciones Científicas)
Videla, M., Mendez, R. A., Clavería, R. M., Silva, J. F., & Orchard, M. E. 2022, AJ, 163, 220
Wales, D. J., & Doye, J. P. K. 1997, JPCA, 101, 5111
Wenger, M., Ochsenbein, F., Egret, D., et al. 2000, A&AS, 143, 9
Wilson, R. H. J. 1976, MNRAS, 177, 645
Zwiers, H. J. 1896, AN, 139, 369